NEUROSCIENCE

X-ray videocystometry for high-speed monitoring of urinary tract function in mice

Jan Franken[1†], Helene De Bruyn[1†], Roma Rietjens[1], Andrei Segal[1], Dirk De Ridder[2], Wouter Everaerts[2], Thomas Voets[1*‡], Greetje Vande Velde[3‡]

Lower urinary tract dysfunction (LUTd) represents a major health care problem with a high, unmet medical need. Design of additional therapies for LUTd requires precise tools to study bladder storage and voiding (dys)function in animal models. We developed videocystometry in mice, combining intravesical pressure measurements with high-speed fluoroscopy of the urinary tract. Videocystometry substantially outperforms current state-of-the-art methods to monitor the urine storage and voiding process, by enabling quantitative analysis of voiding efficiency, urethral flow, vesicoureteral reflux, and the relation between intravesical pressure and flow, in both anesthetized and awake, nonrestrained mice. Using videocystometry, we identified localized bladder wall micromotions correlated with different states of the filling/voiding cycle, revealed an acute effect of TRPV1 channel activation on voiding efficiency, and pinpointed the effects of urethane anesthesia on urine storage and urethral flow. Videocystometry has broad applications, ranging from the elucidation of molecular mechanisms of bladder control to drug development for LUTd.

INTRODUCTION

An estimated 1 billion people worldwide suffer from some form of lower urinary tract dysfunction (LUTd) (*1*, *2*). This includes a broad spectrum of conditions in which the apparently simple process of urine storage and voiding is disturbed. It can manifest as urinary incontinence, nocturia, the inability to efficiently empty the bladder, permanent urgency, or obstructive voiding (*3*, *4*). LUTd is a common comorbidity of diabetes and various neurodegenerative diseases and its prevalence increases with aging. Although generally not life-threatening, LUTd is often detrimental to the patient's quality of life and productivity. The societal costs are accordingly high (*1*). Current pharmacotherapies for LUTd mainly target contractility of the smooth muscle and urethra. They often lack long-term efficacy and regularly produce side effects, both leading to low patient compliance. There is thus a high need for additional treatment options for LUTd, which inevitably requires better insights into the fundamental mechanisms and molecular players that determine bladder (patho)physiology (*4*).

Cystometry in rodents has been broadly used to serve this purpose (*5*). It is a well-described technique where the bladder is simultaneously filled and intravesical pressure (P_{ves}) measured through a transurethral or implanted catheter. In combination with specific pharmacological tools and genetic approaches in healthy and diseased rodent models, it has shown its merits by identifying key cellular processes and molecular players that regulate bladder (patho) physiology (*4*, *6*–*9*).

Nevertheless, the absence of quantitative information regarding the filling state of the bladder, localized movements of the bladder wall, urethral function, or vesicoureteral reflux (VUR)—all essential aspects of LUTd in patients—strongly limit the usefulness of cystometry to study bladder dysfunction in rodents. Various valuable complementary approaches have been applied, including the implantation of stretch/movement sensors in the bladder wall, quantitation of urine output using balances or optical imaging of urine spots, ultrasound-based measurements of bladder volume (V_{ves}) and urine flow, and electromyography of urethral sphincter muscle (*7*, *8*, *10*–*12*). However, these approaches either do not offer the ability to measure V_{ves} and urine flow with sufficient precision and temporal resolution or require invasive/obtrusive interventions that alter the physiological process of interest and preclude a broad applicability, especially in freely moving animals.

These shortcomings motivated us to develop videocystometry, combining cystometry with concurrent high-speed and high-resolution imaging of the lower urinary tract in mice. Videocystometry allows for noninvasive monitoring of key parameters of bladder and urethral function that were previously inaccessible, both in anesthetized and awake, freely moving mice. We provide several illustrations of the previously unattainable possibilities offered by videocystometry, including the discovery of an acute effect of TRPV1 activation on voiding efficiency ($E_{voiding}$), the first quantitative in vivo observations of localized micromotions of the bladder wall and of VUR, and the elucidation of profound effects of urethane anesthesia on urine storage and urethral flow. The ease-of-use and easy application of videocystometry also opens opportunities for noninvasive, fast, and highly accurate volume measurement in other hollow organs or structures.

RESULTS

Establishment of videocystometry

Because classic cystometry in mice allows accurate measurements of P_{ves} but provides no direct evidence on V_{ves} or urethral flow, we set out to complement the technique with time-resolved imaging of the LUT. To achieve this, we supplemented the intravesical solution used for cystometry in mice with the iodinated contrast agent iomeprol (50%), established that the contrast agent does not affect basal cystometric parameters (fig. S1, A to C), and imaged the LUT using

[1]Laboratory of Ion Channel Research (LICR), VIB-KU Leuven Centre for Brain and Disease Research, Department of Cellular and Molecular Medicine, KU Leuven, Leuven, Belgium. [2]Laboratory of Organ System, Department of Development and Regeneration, KU Leuven, Leuven, Belgium. [3]Biomedical MRI, Department of Imaging and Pathology, KU Leuven, Leuven, Belgium.
*Corresponding author. Email: thomas.voets@kuleuven.vib.be
†These authors contributed equally to this work.
‡These authors contributed equally to this work as co–senior authors.

x-ray–based videofluoroscopy (Fig. 1A). We refer to this combined technique as videocystometry. Note that the approach is technically analogous to videourodynamics, which is used in urological clinical practice for the diagnosis of LUTd in selected patients (*13*). A key difference is that we imaged mice at video rate for the entire duration of the videocystometry experiments, whereas during videourodynamics in patients, only a few x-ray images ("snap shots") can be taken to minimize radiation damage (*13*). We initially established videocystometry in urethane-anesthetized mice (Figs. 1 to 5) and subsequently demonstrated the feasibility of the technique in awake, unrestrained mice (Fig. 6), which could be imaged either from the top (as shown in Fig. 1A) or from the side. Videocystometry provides precise information on clinically relevant parameters of LUT function that could not be addressed using classic cystometry or other techniques used in preclinical bladder research.

A first set of parameters relates to volume alterations during urine storage and voiding. Common LUTds such as overactive or underactive bladder change the maximal functional capacity of the bladder. Moreover, incomplete emptying of the bladder leads to residual urine, which is associated with increased risk of bladder infections and stone formation (*2*, *3*). Our approach to monitor V_{ves} is based on the attenuation of the x-rays passing through the mouse abdomen. We found that the background-corrected x-ray opacity in

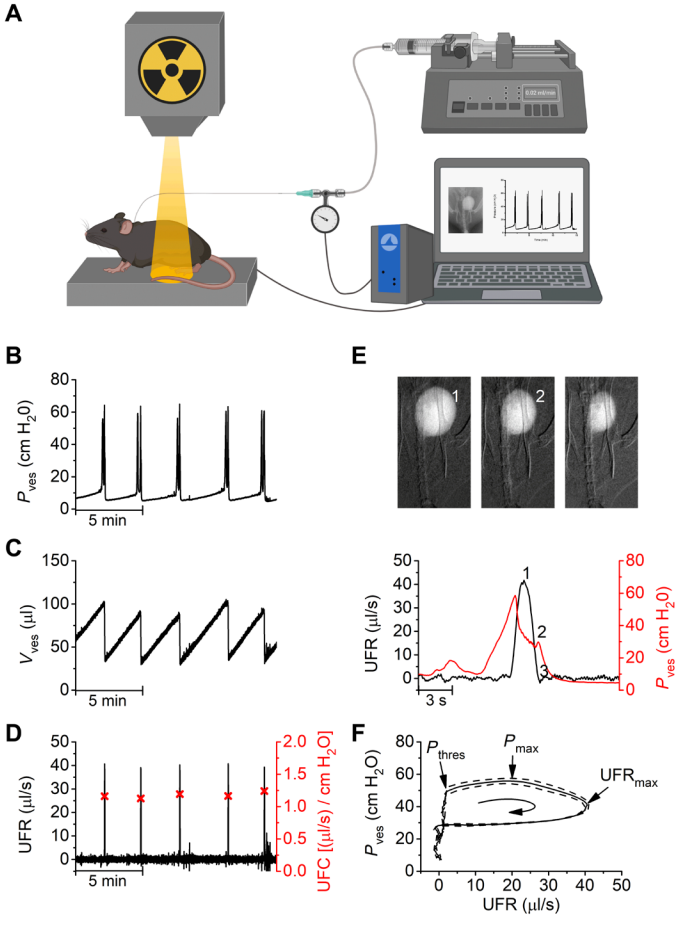

Fig. 1. Monitoring lower urinary tract function in mice using videocystometry. (**A**) Videocystometry setup, combining pressure measurements obtained with classic cystometry and video-rate x-ray–based fluoroscopy. (**B** to **D**) Quantitative videocystometry output measures, including the time course of changes in P_{ves} (B), V_{ves} (C), and urethral flow rate (UFR; D) during a 15-min segment of an experiment. In (D), the peak urethral flow conductance (UFC) during individual voids is indicated. (**E**) Zoomed-in illustration of the time course of P_{ves} and UFR during a single void with corresponding background-subtracted fluoroscopy images taken at the time points indicated. (**F**) Mean pressure-flow curve obtained by averaging P_{ves} and UFR segments as shown in (E), aligned at the peak UFR. See also movie S1.

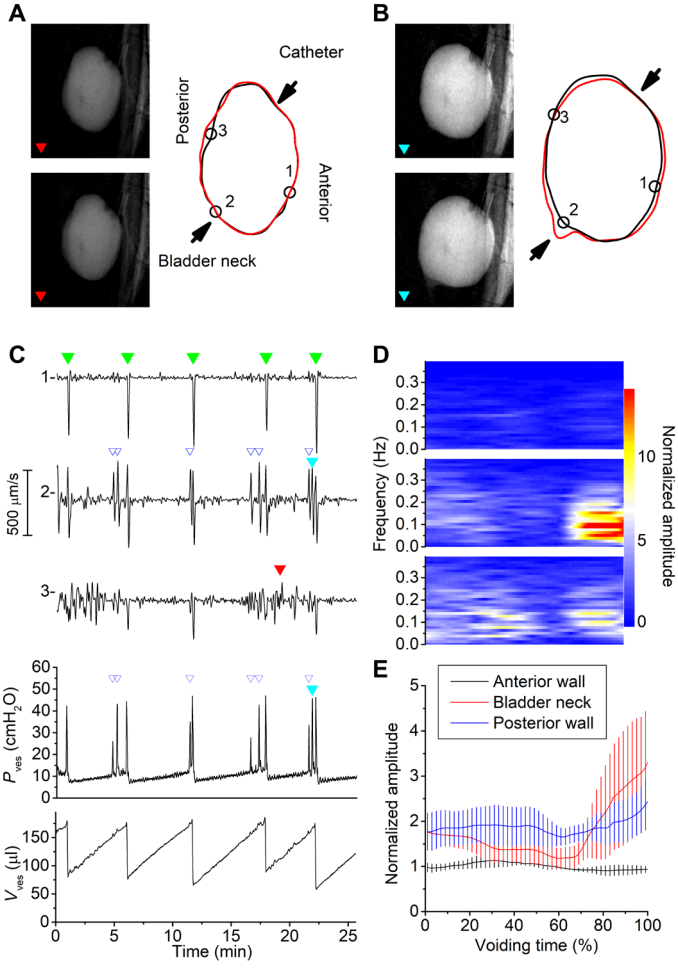

Fig. 2. Videocystometry for the analysis of bladder micromotions. (**A** and **B**) Fluoroscopy images imaged from the lateral side (left) and corresponding bladder circumference (right) illustrating two types of micromotions of the bladder wall: movement of the posterior wall (A) and movement around the bladder neck (B). (**C**) Time course of the radial velocity of the three border points shown in (A) and (B), P_{Ves} and V_{Ves}. Time points of individual voids are indicated with solid green triangles, nonvoiding contractions with open blue triangles, and the two events shown in (A) and (B) with filled red and cyan triangles. (**D** and **E**) Spectral analysis of bladder wall velocity during the filling phase. In (D), mean spectrograms of the movement of the three indicated bladder points during the filling phase are shown. Short-time Fourier transform analysis was used to produce spectrograms for individual filling periods, which started immediately after one void (voiding time, 0%) and ended just before the next void (voiding time, 100%), and averaged. In (E), the amplitude of the mean spectrograms of $n = 5$ animals in the spectrum band between 0.05 and 0.2 Hz is shown, normalized to the mean amplitude in the anterior wall. See also movie S2 and fig. S5.

our experimental setting is linearly related to the volume of intravesical contrast solution between x-ray generator and detector, both in a test tube setup and in vivo (fig. S1, D and E). Thus, by continuously measuring the opacity in a region of interest encompassing the bladder, we were able to monitor V_{ves}, concurrent with cystometric determination of P_{ves} during successive filling and voiding cycles in mice (Fig. 1, B and C, and movie S1; see Materials and Methods). To assess the accuracy of these measurements, we performed a set of control experiments. At the end of each videocystometry protocol, the entire bladder content was collected into a test tube and weighed, providing an independent and precise measure (ground truth) of the V_{ves} at that time point (fig. S2). Values for V_{ves} determined by videocystometry showed a high accuracy [104.8 ± 8.5% of the ground truth (means ± SD); Pearson's correlation coefficient = 0.9922; $n = 27$] (fig. S2C). In contrast, when V_{ves} was estimated from urine drops using the standard gravimetric technique (fig. S2, A and B), accuracy was low and mostly showed an overestimation of actual V_{ves} (266.1 ± 165.8% of the ground truth; Pearson's correlation coefficient = 0.1291; $n = 8$) (fig. S2C). Videocystometry thus allows for accurate and noninvasive determination of the functional bladder capacity (BC; the V_{ves} just before voiding), residual volume (RV; the volume immediately after a void), and $E_{voiding}$ [$E_{voiding} = (1 - RV/BC) \times 100\%$; the fraction of the bladder content that is expelled during a void] for every individual void. In urethane-anesthetized mice, we obtained average values for BC and RV of 126.7 ± 29.8 µl and 63.6 ± 26.8 µl, respectively, indicating a consistent incomplete emptying of the bladder. The average $E_{voiding}$ amounted to 48.4 ± 15.8% (see also Fig. 6).

A second set of parameters relates to flow of urine through the urethra during voiding. Reduction in urethral flow is a common symptom in males with bladder outlet obstruction due to benign prostatic enlargement, in neurogenic bladder patients with detrusor sphincter dyssynergia or in patients with urethral stricture disease (*2*, *3*). The high frame rate (up to 30 Hz) of the fluoroscopy-based volume measurements allowed precise determination of the urethral flow rate (UFR) during voiding, as the negative time derivative of the V_{ves} ($UFR = -dV_{ves}/dt$; Fig. 1D). In anesthetized mice, this analysis yielded a typical bell-shaped flow pattern during a void, with a peak UFR of 28.0 ± 6.7 µl/s (Fig. 1E). Precise synchronization of P_{ves} and UFR measurements also allowed to construct pressure-flow curves, which represent a central diagnostic tool to evaluate urethral dysfunction in clinical practice in humans (Fig. 1F). From these pressure-flow curves, one can directly read the pressure at which the void is initiated (P_{thres}), representing the point at which the P_{ves} exceeds the pressure applied by the urethral sphincter, and appreciate that the flow peak is delayed relative to the maximal P_{ves} (P_{max}). Moreover, the simultaneous pressure and flow measurements enable determination of the time course of the urethral flow conductance ($UFC = UFR/P_{ves}$) (Fig. 1D). The peak UFC during a void amounted to 0.71 ± 0.19 µl/s per cmH_2O. Note that, while we did most of our experiments using female mice, the approach is equally applicable to male mice, and we did not find any significant difference between both sexes for parameters related to pressure, volume, $E_{voiding}$, or urethral flow (fig. S3). Likewise, videocystometry can also readily be adapted to larger animals such as rats (fig. S4), provided that the dimensions of the x-ray detector allow imaging of the entire lower abdomen.

Additional information provided by videocystometry relates to local movements of the bladder wall. Local contractions/elongations of the bladder wall, also known as bladder micromotions, have been suggested to play an important role in physiological sensing of the filling state of the bladder and in the pathology of detrusor overactivity (*14*, *15*). However, up to date, these micromotions could only be studied ex vivo in isolated whole bladder or bladder strip preparations (*14*, *15*). During videocystometry, especially when imaging from the lateral side of the animal, we frequently observed movement of segments of the bladder wall during the bladder filling phase (Fig. 2, A and B, and movie S2). To quantitatively describe this local movement of the bladder wall in vivo, we developed a border-tracking algorithm to identify the position of multiple border points on the bladder wall from fluoroscopy images and determined their distance from the center of the bladder in function of time. The time derivative of the distance of these individual border points relative to the center of the bladder (i.e., the radial velocity) provides a measure for local movement, which can be temporally aligned with P_{ves} and V_{ves} (Fig. 2, A to C, and fig. S5). From these movement data, time-frequency power spectrograms were constructed for different areas of the bladder wall, allowing straightforward visualization of the timing, magnitude, and characteristic frequency of localized movement. By aligning the spectrograms to the start and end of individual filling/voiding cycles, we calculated average spectrograms during bladder filling in different areas of the bladder wall (Fig. 2D). This approach allows for precise identification of areas where micromotions occur and how their movement correlates with the filling state of the bladder. This analysis revealed notable differences in local movement between the posterior and anterior wall and the area around the bladder neck. In particular, the posterior wall showed a much higher level of movement during the entire filling phase compared to the anterior wall, and these movements did not noticeably correlate with events in the pressure trace (Fig. 2, A and C to E, and fig. S5). In the region of the bladder neck, we observed increasing movement during the later phase of the filling cycle (Fig. 2, D and E), which could also be visually appreciated as the transient opening of the internal sphincter, without urine loss (Fig. 2B). These movements of the bladder neck were tightly correlated with nonvoiding contractions detected in the pressure trace (Fig. 2C).

Of note, the automated identification of the points on the bladder wall also provided a second, intensity-independent estimate of V_{ves}, which we refer to as $V_{ves,spheroid}$. $V_{ves,spheroid}$ was calculated assuming that the shape of the mouse bladder can be approximated as a spheroid with the line connecting the border points at the bladder neck and at the site of catheter implantation as symmetry axis. Overall, we found $V_{ves,spheroid}$ to be in good agreement with the intensity-based V_{ves} estimates, except for the first voids, when the bladder likely still contains urine without contrast solution (fig. S6). We also compared $V_{ves,spheroid}$ at the end of experiments with collected and weighed bladder content (ground truth) at that time point (fig. S2), revealing an excellent accuracy [100.8 ± 24.1% of the ground truth (means ± SD); Pearson's correlation coefficient = 0.9323; $n = 11$]. $V_{ves,spheroid}$ thus provides an alternative means to estimate V_{ves} in mice under conditions where accurate intensity-based volume estimates are not feasible, for instance, due to movement-induced changes in background opacity in awake, moving animals (see Fig. 6). We note that the correlation with the weighed bladder content is lower for $V_{ves,spheroid}$ than for V_{ves} (fig. S2), possibly due to inter-animal variability in the accuracy of the spheroid approximation.

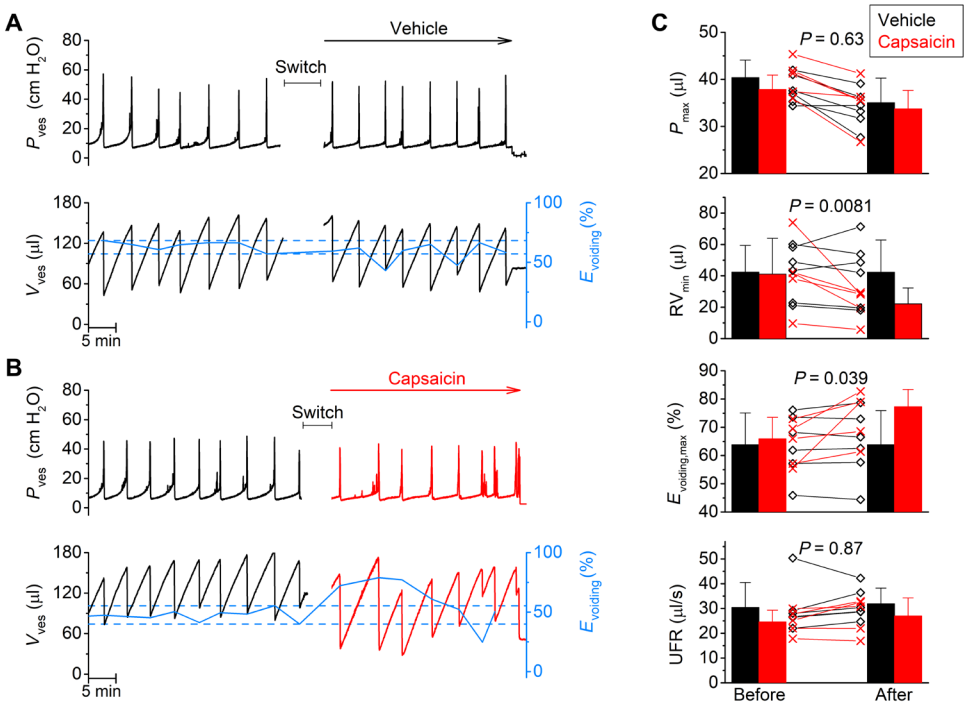

Fig. 3. Videocystometry reveals the acute effect of TRPV1 activation of $E_{voiding}$. (**A** and **B**) Pressure and volume traces comparing the effects of intravesical administration of vehicle (A) or the TRPV1 agonist capsaicin (100 µM; B). After a baseline period of 30 min, the intravesical perfusion solution was switched to a solution containing either vehicle or capsaicin. During the switch, recording was stopped during the indicated times. The solid blue line connects the $E_{voiding}$ for individual voids. Dotted lines indicate the lowest and highest $E_{voiding}$ during the baseline period. (**C**) Comparison of videocystometry parameters before and after the switch to either vehicle or capsaicin. Bar charts indicate means ± SD, with data points from individual animals shown along. RV_{min} and $E_{voiding,max}$ represent the single lowest residual volume (RV) and single largest $E_{voiding}$, respectively, recorded before and after the switch. Statistical comparison of the relative change of the indicated parameters (after/before) between capsaicin-treated ($n = 5$) and vehicle-treated ($n = 6$) animals was performed using a two-tailed, unpaired t test. Values for the relative changes (after/before × 100%; vehicle versus capsaicin) were as follows: P_{max}, 89.1 ± 8.3 versus 86.6 ± 8.4%; RV_{min}, 97.0 ± 6.5 versus 57.4 ± 6.8%; $E_{voiding,max}$, 99.7 ± 0.3 versus 115.7 ± 7.2%; UFR, 107.6 ± 5.4 versus 109.0 ± 6.4%.

Acute TRPV1-dependent changes in V_{ves} and $E_{voiding}$

Next, we used videocystometry to evaluate the effect of intravesical drug application, using TRPV1, a nociceptor channel expressed on sensory nerve endings in the bladder wall, as molecular target. Earlier studies indicate that TRPV1 plays a role in afferent signaling from the bladder, and small molecules that either inhibit or activate and subsequently desensitize TRPV1 have been used in preclinical and clinical studies to treat bladder dysfunction (*4*, *16*–*18*). However, the acute effects of TRPV1 activation on bladder voiding and $E_{voiding}$ are poorly understood.

We performed videocystometry and, after a baseline period of 30 min, the mouse bladder was instilled with an infusion solution supplemented with either capsaicin, a potent and selective TRPV1 activator or its vehicle for another 30 min. Figure 3 (A and B) shows the corresponding videocystometric time course of P_{ves} and V_{ves}, comparing the effect of intravesical administration of vehicle versus capsaicin. These experiments revealed a pronounced but transient reduction of the RV and a significant increase in $E_{voiding}$ in the first 10 min following capsaicin infusion (Fig. 3C). Note that this acute effect of TRPV1 activation on voiding would be missed when using classical cystometry, because no significant differences were observed between capsaicin- and vehicle-treated animals with regard to pressure-based parameters (Fig. 3C).

$E_{voiding}$ and urethral conductance in a bladder outlet obstruction model

As shown in Fig. 1, videocystometry allows the precise measurement of the UFR and UFC and the construction of pressure-flow curves. To illustrate the applications of these analytical concepts, we used videocystometry to quantify the consequences of a severe, transient, and artificial bladder outlet obstruction. After a baseline period of normal filling/voiding cycles during 20 min, a Ch 14 Foley catheter was inserted into the mouse vagina for a period of 20 min. Next, the catheter was removed and videocystometry was performed for another 20 min. Bladder obstruction caused a pronounced and reversible reduction in the peak UFR and UFC, increased RV, and a strong decrease in $E_{voiding}$ (Fig. 4, A to E, and movie S3). These were accompanied by an increased maximal pressure and voiding frequency. Furthermore, the obstruction induced a pronounced shift of the pressure-flow curves, akin to the changes observed in patients with bladder outlet obstruction. After removal of the obstruction, all measurements returned to the preobstruction levels. These findings indicate that videocystometry enables detailed and quantitative detection of changes in urethral function in mice, which could not be addressed by cystometry or other available techniques, paving the way for further investigations into the molecular mechanisms and pharmacological treatment of bladder outlet dysfunction.

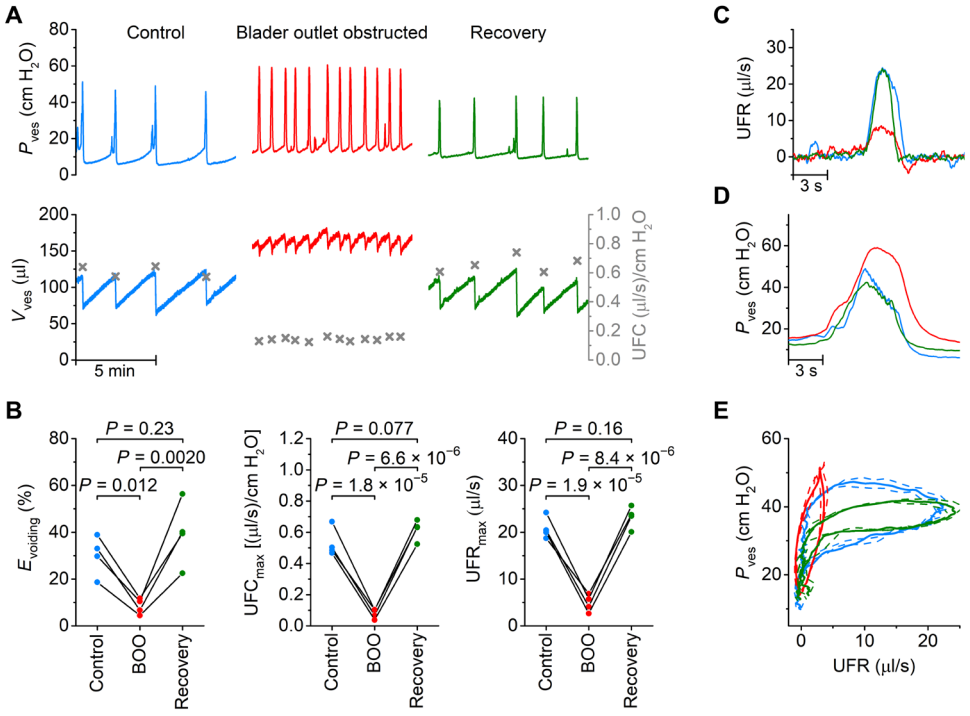

Fig. 4. Videocystometry provides detailed quantification of urethral obstruction. (**A**) Representative videocystometry experiment showing the reversible effect of bladder outlet obstruction (BOO) on P_{ves}, V_{ves}, and UFC. (**B**) Comparison of videocystometry parameters before (control; blue traces), during BOO (red traces) and after recovery (green traces). Statistical analysis was performed using one-way repeated measures analysis of variance (ANOVA) ($n = 4$). (**C** and **D**) Zoomed-in example of UFR and P_{ves} during single voids before, during, and after obstruction. (**E**) Average pressure-flow trace (±SEM) for the experiment shown in (A), illustrating the reversible change in flow pattern induced by urethral obstruction. See also movie S3.

Quantitative analysis of VUR

Backflow of urine into the kidney, known as VUR, is associated in humans with pyelonephritis and kidney dysfunction (*19*). The current standard method to evaluate VUR in mice entails the qualitative assessment of pressure-induced flux of dye from the bladder to the kidneys in euthanized animals (euthanized cystogram) (*20*, *21*). Whereas this approach has allowed detecting variable degrees of VUR in several inbred and genetically modified mice (*21*–*24*), it does not allow assessment of VUR during normal bladder filling/voiding cycles, and death may affect the parameters that determine reflux.

While performing videocystometry, we occasionally (in about 20% of the animals) observed mice in which the volume of the bladder increased sublinearly, despite constant fluid infusion and absence of signs of leakage or transurethral fluid loss. A typical example is shown in Fig. 5. Notably, the sublinear increase in V_{ves} was associated with measureable attenuation of the x-ray signal craniodorsally of the bladder (Fig. 5A), and image differencing revealed clear filling of the kidneys with contrast solution (Fig. 5A). The time-dependent changes in x-ray attenuation in regions of interest encompassing the bladder and kidney, respectively, allowed simultaneous monitoring of the V_{ves} and of the volume of intravesical fluid that reached the kidneys (V_{kidney}) through VUR (Fig. 5A). As shown in this example, intravesical fluid starts flowing to the kidney in the later phase of the bladder filling cycle when P_{ves} is elevated; V_{kidney} reaches a maximum during the void and gradually flows back to the bladder when P_{ves} returns to baseline following a void (Fig. 5, A and B). We also calculated the rate of fluid flux from the bladder to the kidney as the derivative of V_{kidney} (ureteral flow rate = dV_{kidney}/dt; Fig. 5C) and found maximal flow rates of up to 1 µl/s just preceding the void. Emptying of the refluxed solution from the kidney following a void, i.e., a negative ureteral flow rate, was delayed relative to the peak UFR (Fig. 5C). The fact that we observed VUR in only a subset of animals is in line with earlier studies indicating that not more than 20% of female C57BL/6J mouse exhibit VUR, when assessed by euthanized cystograms (*24*). These findings demonstrate that videocystometry allows the quantitative analysis of VUR in alive mice, opening the way to further studies on the underlying mechanisms and relation to LUT infections.

Videocystometry in freely moving mice

Last, we provide proof of principle that videocystometry is feasible in awake, nonrestrained mice. For these experiments, mice were placed in a small container, in which they were able to move around while remaining within the range of the imaging detector (movie S4). Because the movement of the animals leads to changes in the background attenuation of the x-ray, continuous intensity-based measurements of V_{ves} were not feasible. Yet, mice are mostly sitting still during voiding, which allowed the accurate measurement of UFR, P_{ves}, and derived parameters during individual voids (Fig. 6A). Moreover, determination of $V_{ves,spheroid}$ allowed volume estimates at any time point on the basis of the bladder outline (Fig. 6A). This set of experiments using awake mice ($n = 5$) revealed pronounced differences in the voiding parameters compared to anesthetized animals. In particular, videocystometry revealed a much lower RV and concurrently a higher $E_{voiding}$ in awake compared to the anesthetized animals (Fig. 6B), whereas $P_{ves,max}$ did not differ significantly (Fig. 6B).

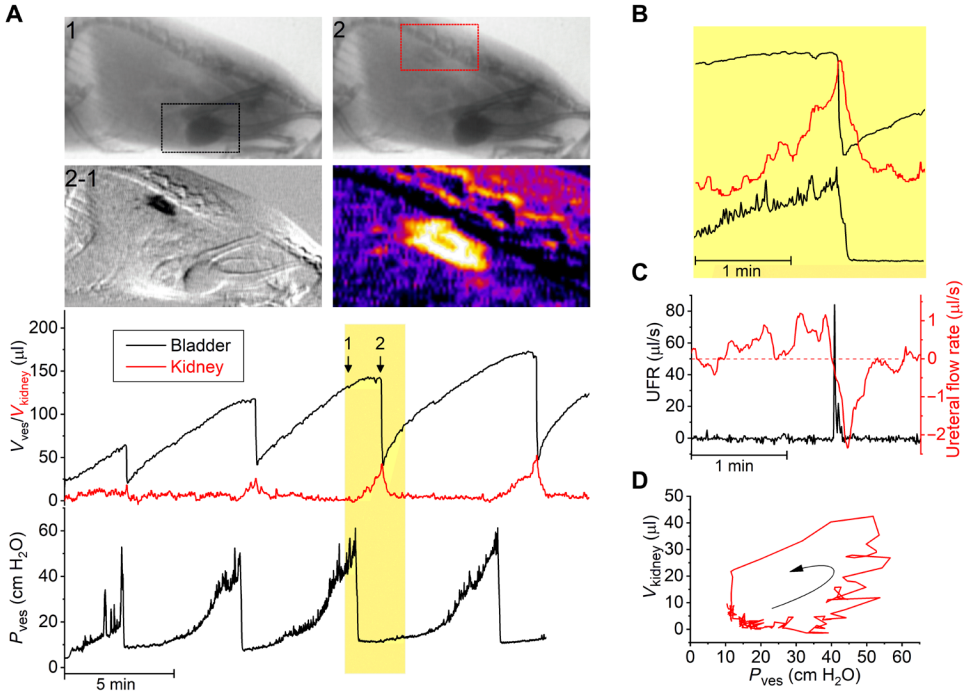

Fig. 5. Videocystometry allows the quantitative in vivo assessment of VUR. (**A**) Videocystometry in an animal exhibiting VUR. The V_{ves} trace shows a sublinear increase in V_{ves} toward the end of the filling phase, which is associated with a visible increase in x-ray opacity in the region of the kidneys. The two top images correspond to the indicated time points before (1) and during (2) reflux to the kidney, whereas the two lower images show the difference image (2-1) and a pseudo-color magnification of the latter, illustrating contrast-containing solution reaching the kidney. Squared areas indicate regions of interest used for volume measurement. Changes in opacity in the kidney region allow measurement of the volume of contrast fluid refluxed to the kidney (V_{kidney}). (**B**) Enlarged view on the changes in V_{ves}, V_{kidney}, and P_{ves} during the indicated void shows that V_{kidney} reaches a maximum during the void, followed by the gradual flow of contrast back to the bladder. (**C**) UFR and ureteral flow rate during the void indicated in (B). (**D**) Volume-pressure trace for the kidney filling and emptying during, illustrating onset of VUR at P_{ves} > ~40 cmH_2O.

We could attribute the more efficient voiding to increased UFR and UFC in awake mice (Fig. 6B). These results indicate that anesthesia negatively affects the relaxation of the urethral sphincters during voiding, resulting in incomplete emptying of the bladder, which is in line with the conclusions from earlier experiments in decerebrate rats (*25*). Awake videocystometry is therefore applicable to evaluate lower urinary tract (dys)function in conscious, nonrestrained animals.

DISCUSSION

Cystometry is now the standard technique to measure lower urinary tract function in small laboratory animals in vivo. It measures changes in P_{ves} during consecutive bladder filling-voiding cycles (*5*, *17*, *26*, *27*). We demonstrate here that complementing classical cystometry with x-ray–based fluoroscopy in mice enables continuous accurate assessment of an extensive set of (patho)physiologically relevant parameters of lower urinary tract function, which were not accessible with existing techniques. In particular, by combining pressure measurements with high-resolution, quantitative imaging of the lower urinary tract at video rate, videocytometry provides unprecedented details about the voiding process, with precise determination of the efficiency of voiding and highly time-resolved measurement of urethral flow and flow resistance. We initially established videocystometry in anesthetized mice and demonstrated its applicability to awake, unrestrained mice.

In earlier work, cystometry is often combined with balance-based measurement of the voided fluid to estimate BC, $E_{voiding}$, and urethral flow (*5*, *11*, *17*). However, this approach lacks the temporal resolution to allow for precise measurements of urethral flow or conductance/resistance. This is, in part, due to surface tension, which induces a lag between actual urine release at the urinary meatus and the time point when the voided urine drops reach the balance. Some improvement in the time resolution was achieved by placing a wick of tissue paper close to the meatus to rapidly catch voided urine but such an approach is not feasible in moving animals (*11*). Similar temporal limitations apply to a recently developed elegant approach to detect urine voiding in freely moving mice using continuous imaging urine spots under ultraviolet illumination (*7*). Moreover, because the V_{ves} in mice is so small, the loss of urine due to adherence to the perineum and evaporation is substantial and inevitably leads to accumulating errors in the estimation of the actual V_{ves} (fig. S2) and consequently $E_{voiding}$. A recent study combined cystometry with a soft strain gauge mounted around the rat bladder, allowing the simultaneous assessment of bladder pressure and shape (*10*). The stretchable strain gauge yields real-time information reporting changes in bladder circumference that occur during filling and emptying of the bladder, at a sampling rate of 0.25 Hz (*10*). While this technique allows indirect measurements of V_{ves} in freely moving animals, a direct conversion of the strain gauge signal to absolute volume is not available, and the temporal resolution is too low to allow detailed flow quantification. Moreover, the dimensions

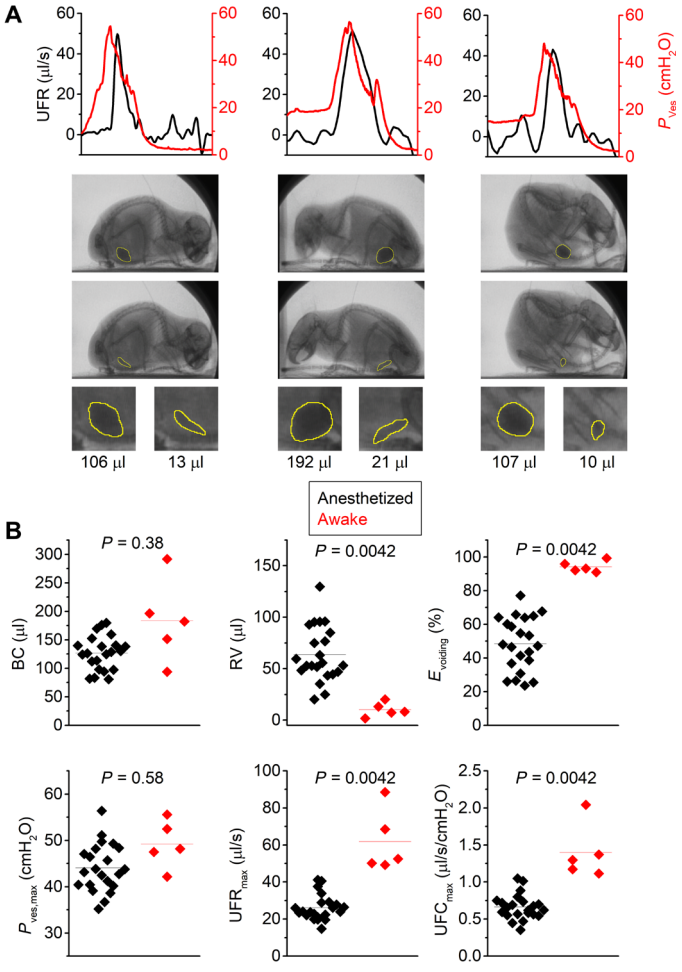

Fig. 6. Videocystometry in awake, nonrestrained mice. (**A**) UFR and P_{ves} traces with corresponding bladder images right before and after voiding in an awake, nonrestrained mouse, enclosed in a small box to ensure that the animal remains within the field of view. Indicated volume refers to $V_{ves,spheroid}$, where the bladder is approximated as a spheroid (see Materials and Methods). (**B**) Comparison of videocystometry parameters between anesthetized ($n = 22$) and awake ($n = 5$) animals. Despite the relatively low number of awake animals in the proof-of-principle experiment, our findings indicate a significantly higher $E_{voiding}$ associated with a higher maximal flow rate. Data in (B) were compared using a Mann-Whitney *U* test. See also movie S4.

of the strain gauge make it difficult to implement this technique in mice. Cystometry has also been combined with bladder ultrasonography, which allowed an estimation of the V_{ves} before and after a void from cross-sectional areas of the bladder (*12*). However, ultrasonography requires the constant pressure of an ultrasound probe against the lower abdomen, which may affect bladder function and is incompatible with measurements in awake animals.

Therefore, we consider that videocystometry, with its highly accurate and time-resolved volume measurements in both anesthetized and awake mice, largely outperforms the current state-of-the-art methods to monitor the urine storage and voiding process. In this study, we presented several illustrations of the potential advantages offered by videocystometry over alternative techniques. First, the accurate and synchronized measurement of P_{ves} and urethral flow allowed us to establish pressure-flow curves in mice, and how these are affected by urethral obstruction. Pressure-flow curves constitute a central diagnostic tool to evaluate urethral dysfunction or detrusor-sphincter dyssynergia in clinical practice in humans, and videocystometry thus opens previously unattainable possibilities to study the pathophysiology of these LUTds in mice. Note that detrusor-sphincter dyssynergia has also been studied in mice using a combination of cystometry with electromyography of the urethral muscle (*8*, *28*). While this latter approach provides synchronized measurements of P_{ves} and electrical activity of the sphincter muscle, it does not provide the detailed information on urethral flow and resistance offered by videocystometry. Second, videocystometry is well suited for the evaluation of the effects of intravesical drugs acting on targets in the bladder wall. As an example, because of the accurate determination of V_{ves}, we were able to detect a transient increase in $E_{voiding}$ upon acute stimulation of the bladder wall with the TRPV1 agonist capsaicin. On the basis of a large body of earlier work, it was already well established that prolonged capsaicin stimulation leads to desensitization of TRPV1-expressing nociceptive afferents (*29*), which has been tested in a clinical setting to reduce bladder activity (*30*). However, the acute effects of TRPV1 activation on bladder function remain incompletely understood. Our findings demonstrate a transient enhancement of $E_{voiding}$ and a reduction of RV upon acute TRPV1 activation. Third, we showed an important difference in $E_{voiding}$ and UFC between awake and anesthetized mice, illustrating the prominent effects of (urethane) anesthesia on LUT function (*25*). In addition to providing synchronized and precise measurements of V_{ves}, P_{ves}, and urethral flow, our findings also illustrate the power of videocystometry to identify and quantitatively describe two other important aspects of bladder (patho) physiology in vivo, namely, bladder wall micromotions and VUR.

Bladder micromotions are spontaneous phasic movements of the bladder wall during urine storage, which have been associated with pathological bladder overactivity (*15*). However, before the present study, the study of micromotions was limited to ex vivo tissue strips and isolated bladder preparations, precluding their analysis during normal bladder filling or correlation with P_{ves} (*14*, *15*). Using videocystometry, we were able to combine P_{ves} measurements with the capturing of the movement of the bladder wall at video rate. This approach not only allowed for the image-based identification of distinct and localized motility of the bladder wall but also enabled a detailed spectral analysis of the movement speed of points at different sites on the bladder wall. Our analysis revealed a higher level of localized movement of the posterior compared to the anterior bladder wall during the filling phase, and these micromotions were generally not correlated with detectable P_{ves} peaks. In the later phase of the filling phase, we observed increased movement in the region of the bladder neck, including transient opening of the internal sphincter, and these movements were tightly correlated with nonvoiding contractions in the pressure trace. While these findings are congruent with current theories about bladder function in humans, local differences in spontaneous activity of the bladder wall in vivo have not been demonstrated to date. Thus, videocystometry provided the first in vivo measurements of bladder micromotions in mice and identified a link between nonvoiding contractions and dilatation of the bladder neck.

In humans, VUR, the retrograde flux of urine from the bladder via the ureters to the renal calyx, can be caused by a congenital defect of the one-way valve at the ureterovesical junction or by increased P_{ves} due to bladder outlet obstruction and represents an

important risk factor for pyelonephritis and chronic kidney disease. Although there are several mouse models of VUR (*21*–*24*), assays to study the pathophysiology of VUR are limited. The current gold-standard assay, the euthanized cystogram, involves the pressure injection of dye in the bladder of euthanized animals, preventing the repetitive assessment of VUR during normal physiological bladder function (*20*, *21*). A semiquantitative in vivo assessment of VUR has been achieved by the trans-urethral infusion of microbubbles into the bladder, followed by ultrasound quantification of the size of the microbubble-filled renal pelvis (*21*). However, this technique is limited to anesthetized mice and does not allow time-resolved assessment of VUR during normal bladder filling/voiding. Our videocystometric experiments not only allowed us to visualize VUR in a subset of the tested mice (~20%, in line with earlier studies using euthanized cystograms in C57BL/6J mice) (*24*) but also enabled a quantitative description of the pressure-dependent filling and emptying of the kidney via the ureters during successive filling-voiding cycles. These findings indicate that videocystometry is well tailored for preclinical studies on the genetic causes and pathophysiology of VUR.

With the fluoroscopy settings used in this study, mice were subjected to x-ray radiation in the order of 300 to 500 μSv/hour, leading to a total dose of <1 mSv for a typical experimental procedure of 1 to 2 hours. These irradiation doses are at least six orders of magnitude below the median lethal dose (LD_{50}) value of ~1 kSv for 30-day mortality in mice (*31*). During the experiments, the x-ray device was protected with shielding panels and a 0.25-mm lead equivalent protective sheet, and the x-ray source was turned off whenever the animal was being manipulated. Measurements at 1 m from the device revealed an exposure of ≤1 μSv/hour, which can be considered safe for the experimenter considering the yearly dose limit for occupational exposure in the European Union of 20 mSv. Therefore, we consider the x-ray irradiation used for videocystometry to be harmless to the animal and safe for the researcher.

In summary, videocystometry provides extensive opportunities to study aspects of lower urinary tract function and dysfunction in mice or other laboratory animals that were poorly accessible with existing assays. Its implementation in academic or biotech environments can be readily achieved using commercially available pressure sensing and fluoroscopy equipment, along with our open-source analysis software. Therefore, videocystometry is well placed to become the method of choice for studies into the molecular mechanisms controlling normal and pathological bladder function and for the development of novel therapies to treat LUTd.

MATERIALS AND METHODS

Animals

Experiments were conducted on 12- to 16-week-old C57BL/6J mice (Janvier) and on 10- to 12-week-old Wistar rats (Janvier). Experiments were performed using female mice, except when indicated (figs. S3 and S4). Animals were housed in filter-top cages in a conventional facility at 21°C on a 12-hour light/12-hour dark with unrestricted access to food and water. Animals were euthanized immediately after the experiments. All animal experiments followed the Institutional Animal Care And Use Committee guidelines and were carried out after approval of the Ethical Committee Laboratory Animals of the Faculty of Biomedical Sciences of the KU Leuven under project numbers P285/2015 and P035/2018.

Surgery and experimental setup

Suprapubic catheter implantation for cystometry was performed as described earlier (*27*). In short, the mice/rats were induced in a chamber with 4 to 5% isoflurane and maintained under anesthesia with 2% isoflurane (Iso-Vet, Dechra Veterinary Products, Bladel, The Netherlands) in 100% oxygen and a PE-50 catheter was implanted into the bladder dome through an abdominal midline incision. The catheter was flushed with the iso-osmolar intravesical contrast solution (291 mosmol/kg), which consisted of 50% iomeprol (510 mg/ml; Iomeron 250, Bracco Imaging Europe, Wavre, Belgium), 21.4% of 0.9% NaCl (Baxter Uromatic, Baxter, Braine-l'Alleud, Belgium), and 28.6% ultrapure water.

At the end of surgery, the anesthetized animals received urethane [1.3 g/kg body weight from the solution (40 mg/ml); Sigma-Aldrich, Diegem, Belgium] diluted in 0.9% NaCl by subcutaneous injection. A lower dose of urethane (0.3 g/kg), supplemented with the nonsteroidal anti-inflammatory drug carprofen for postoperative analgesia (5 mg/kg; Zoetis, Louvain-la-neuve, Belgium), was used for awake videocystometry. At this dose, which is >5-fold below the LD_{50}, urethane induced only mild sedation, which facilitated videocystometry in nonrestrained animals within the recording chamber (3 cm by 7 cm; height 4 cm). Animals were allowed to recover for at least 30 min from isoflurane anesthesia. Anesthetized or awake animals were placed in an x-ray imaging device on top of a radiolucent infrared heating pad (Quality Heating, Heiloo, The Netherlands). The PE-50 catheter was connected to a pressure sensor and to an infusion pump through a three-way stopcock. Cystometry was performed with infusion of the intravesical contrast solution at a rate of 20 μl/min (mice) or 100 μl/min (rats). Simultaneously, pressure measurements were performed using a TSD104A transducer plugged into a DA100C transducer amplifier connected to a BIOPAC MP150 data acquisition system (BIOPAC Systems Inc., Goleta USA). When indicated, the intravesical contrast solution was supplemented with 100 μM capsaicin (Sigma-Aldrich, Overijse, Belgium) from a 100 mM stock solution in ethanol or with ethanol vehicle. Reversible bladder outlet obstruction was achieved by insertion of a Ch 14 Foley catheter (Rüsch, Teleflex Medical Europe Ltd., Dublin, Ireland) into the vagina.

A set of pilot experiments to assess the feasibility of the videocystometry approach in mice and rats was performed in a μCT Skyscan 1076 (Bruker), which has a maximal frame rate of 1.56 fps, with the field of view centered on and limited to the pelvic region. All later experiments were performed using a LabScope (Glenbrook Technologies, New Jersey, USA), a small-animal fluoroscopy system, which allowed a maximal frame rate of 29.97 fps. Settings used for Skyscan 1076 were 50 kV, 200-μA source current, 35-μm isotropic resolution, 120-ms exposure time, and 0.5-mm Al filter. Settings used for the LabScope fluoroscopy system were 23 kV, 200 μA, and 0.54-mm Al filter. AcqKnowledge 5.0.4 software (BIOPAC Systems Inc., Goleta, USA) was used for the synchronized sampling of pressure data and images.

Data processing and analysis

Fluoroscopy images were loaded into Fiji (ImageJ) (*32*) and inverted (to obtain images where intensity increases with increasing opacity), and the background signal (consisting of averaged images before infusion of the contrast solution) was subtracted. The opacity in function of time of a region of interest encompassing the bladder region (O_{ves}) is linearly related to V_{ves}

$$V_{ves} = k \times O_{ves} \quad (1)$$

The conversion constant k was derived for each experiment as

$$k = \frac{R_{infusion}}{\left(\frac{\Delta O_{ves}}{\Delta t}\right)_{filling}} \quad (2)$$

where the $R_{infusion}$ is the infusion rate (20 µl/min), set by the infusion pump, and $\left(\frac{\Delta O_{ves}}{\Delta t}\right)_{filling}$ is the mean rate of opacity increase during the linear bladder filling period.

As an internal control, the mouse bladder was emptied after each experiment and the residual urine was collected, weighed, and converted to volume taking into account the density of contrast solution of 1.315 g/ml. As shown in fig. S2, these values agreed excellently with the estimated V_{ves} at that time point.

In a subset of experiments, we observed a flattening of the $O_{bladder}$ curve, despite the continuous $R_{infusion}$. As illustrated in Fig. 5, this flattening was associated with increased opacity in the renal region and identified as VUR. The volume of the infusion fluid that reached the kidneys was then obtained from a second region of interest encompassing the kidneys.

UFR was calculated as the negative derivative of V_{ves}

$$UFR = -\frac{dV_{ves}}{dt} \quad (3)$$

or

$$UFR = -\frac{k\,dO_{ves}}{dt} \quad (4)$$

Note that the latter equation can be used to determine UFR, even when the background subtraction of images with an empty bladder is not feasible, such as in awake and freely moving videocystometry. The synchronized measurement of UFR and P_{ves} allowed the construction of pressure-flow plots and the calculation of UFC as UFR/P_{ves}.

We used Igor Pro 8 (WaveMetrics, Lake Oswego, OR, USA) to develop the analytical tool VCA, which includes a user interface and all routines to calculate V_{ves}, UFR, and UFC from fluoroscopy images and pressure traces. VCA also contains a void finder routine that automatically detects voiding events as peaks in the UFR trace and calculates BC, RV, $E_{voiding}$, and pressure-flow curves for each individual peak. Last, the VCA tool includes a border-tracking algorithm that analyzes the position of multiple border points on the bladder wall from fluoroscopy images. For the experiments such as those shown in Fig. 2 and fig. S5, 32 border points were determined, which when connected divide the bladder in 32 sectors with equal central angle. We defined the radial velocity as the time derivative of the distance of these individual border points from the center of the bladder. Short-time Fourier transform analysis was used to produce spectrograms of the movement of the individual bladder points during the filling and voiding phase. Average spectrograms of the filling phase were obtained by aligning the spectrograms to the start and end of individual filling cycles, cutting out the actual voiding events.

On the basis of the identified border points, an intensity-independent measurement of the V_{ves} ($V_{ves,spheroid}$) was obtained, assuming that the bladder can be approximated as a spheroid with the line connecting the border point at the bladder neck and at the site of catheter implantation as symmetry axis

$$V_{ves,spheroid} = \frac{\pi}{6}AB^2 \quad (5)$$

where A and B are the lengths of two diameters, with A connecting border point at the bladder neck and at the site of catheter implantation and B perpendicular to A.

Statistics

Statistical analysis and graphing was performed in OriginPro 9.0 (OriginLab Corporation, Northampton, MA, USA). The Shapiro-Wilk test was used to assess normality of the data. The different parametric and nonparametric tests used are indicated in the legends. Except where indicated otherwise, all summary data are reported as means ± SD. Animals were randomly assigned to one of the different experimental conditions. All measurements were performed on distinct animals; no animals were used in multiple experiments. Whenever possible (Fig. 3), observers were blinded to the treatment conditions. Analysis was performed automatically, obviating the need for blinding.

SUPPLEMENTARY MATERIALS

Supplementary material for this article is available at http://advances.sciencemag.org/cgi/content/full/7/30/eabi6821/DC1

REFERENCES AND NOTES

1. K. S. Coyne, A. Wein, S. Nicholson, M. Kvasz, C. I. Chen, I. Milsom, Economic burden of urgency urinary incontinence in the United States: A systematic review. *J. Manag. Care Pharm.* **20**, 130–140 (2014).
2. J. Franken, P. Uvin, D. De Ridder, T. Voets, TRP channels in lower urinary tract dysfunction. *Br. J. Pharmacol.* **171**, 2537–2551 (2014).
3. D. Griffiths, Neural control of micturition in humans: A working model. *Nat. Rev. Urol.* **12**, 695–705 (2015).
4. M. Vanneste, A. Segal, T. Voets, W. Everaerts, Transient receptor potential channels in sensory mechanisms of the lower urinary tract. *Nat. Rev. Urol.* **18**, 139–159 (2021).
5. M. O. Fraser, P. P. Smith, M. P. Sullivan, D. E. Bjorling, L. Campeau, K. E. Andersson, M. Yoshiyama, Best practices for cystometric evaluation of lower urinary tract function in muriform rodents. *Neurourol.Urodyn.* **39**, 1868–1884 (2020).
6. T. Gevaert, J. Vriens, A. Segal, W. Everaerts, T. Roskams, K. Talavera, G. Owsianik, W. Liedtke, D. Daelemans, I. Dewachter, F. Van Leuven, T. Voets, D. De Ridder, B. Nilius, Deletion of the transient receptor potential cation channel TRPV4 impairs murine bladder voiding. *J. Clin. Invest.* **117**, 3453–3462 (2007).
7. J. A. Keller, J. Chen, S. Simpson, E. H.-J. Wang, V. Lilascharoen, O. George, B. K. Lim, L. Stowers, Voluntary urination control by brainstem neurons that relax the urethral sphincter. *Nat. Neurosci.* **21**, 1229–1238 (2018).
8. K. L. Marshall, D. Saade, N. Ghitani, A. M. Coombs, M. Szczot, J. Keller, T. Ogata, I. Daou, L. T. Stowers, C. G. Bonnemann, A. T. Chesler, A. Patapoutian, PIEZO2 in sensory neurons and urothelial cells coordinates urination. *Nature* **588**, 290–295 (2020).
9. P. Uvin, J. Franken, S. Pinto, R. Rietjens, L. Grammet, Y. Deruyver, Y. A. Alpizar, K. Talavera, R. Vennekens, W. Everaerts, D. De Ridder, T. Voets, Essential role of transient receptor potential M8 (TRPM8) in a model of acute cold-induced urinary urgency. *Eur. Urol.* **68**, 655–661 (2015).
10. A. D. Mickle, S. M. Won, K. N. Noh, J. Yoon, K. W. Meacham, Y. Xue, L. A. McIlvried, B. A. Copits, V. K. Samineni, K. E. Crawford, D. H. Kim, P. Srivastava, B. H. Kim, S. Min, Y. Shiuan, Y. Yun, M. A. Payne, J. Zhang, H. Jang, Y. Li, H. H. Lai, Y. Huang, S.-I. Park, R. W. Gereau IV, J. A. Rogers, A wireless closed-loop system for optogenetic peripheral neuromodulation. *Nature* **565**, 361–365 (2019).
11. P. P. Smith, G. A. Kuchel, Continuous uroflow cystometry in the urethane-anesthetized mouse. *Neurourol.Urodyn.* **29**, 1344–1349 (2010).
12. K. Takezawa, M. Kondo, H. Kiuchi, T. Soda, T. Takao, Y. Miyagawa, A. Tsujimura, N. Nonomura, S. Shimada, Combination of bladder ultrasonography and novel cystometry method in mice reveals rapid decrease in bladder capacity and compliance in LPS-induced cystitis. *Am. J. Physiol. Renal Physiol.* **307**, F234–F241 (2014).
13. M. Wyndaele, P. F. W. Rosier, Basics of videourodynamics for adult patients with lower urinary tract dysfunction. *Neurourol.Urodyn.* **37**, S61–S66 (2018).
14. B. Chakrabarty, D. A. Bijos, B. Vahabi, F. Clavica, A. J. Kanai, A. E. Pickering, C. H. Fry, M. J. Drake, Modulation of bladder wall micromotions alters intravesical pressure activity in the isolated bladder. *Front. Physiol.* **9**, 1937 (2018).

15. M. J. Drake, A. Kanai, D. A. Bijos, Y. Ikeda, I. Zabbarova, B. Vahabi, C. H. Fry, The potential role of unregulated autonomous bladder micromotions in urinary storage and voiding dysfunction; overactive bladder and detrusor underactivity. *BJU Int.* **119**, 22–29 (2017).
16. P. Sadananda, M. J. Drake, J. F. Paton, A. E. Pickering, An exploration of the control of micturition using a novel in situ arterially perfused rat preparation. *Front. Neurosci.* **5**, 62 (2011).
17. R. K. Pandita, M. Fujiwara, P. Alm, K. E. Andersson, Cystometric evaluation of bladder function in non-anesthetized mice with and without bladder outlet obstruction. *J. Urol.* **164**, 1385–1389 (2000).
18. L. A. Birder, Y. Nakamura, S. Kiss, M. L. Nealen, S. Barrick, A. J. Kanai, E. Wang, G. Ruiz, W. C. De Groat, G. Apodaca, S. Watkins, M. J. Caterina, Altered urinary bladder function in mice lacking the vanilloid receptor TRPV1. *Nat. Neurosci.* **5**, 856–860 (2002).
19. S. Swerkersson, U. Jodal, R. Sixt, E. Stokland, S. Hansson, Relationship among vesicoureteral reflux, urinary tract infection and renal damage in children. *J. Urol.* **178**, 647–651 (2007).
20. I. J. Murawski, I. R. Gupta, Vesicoureteric reflux and renal malformations: A developmental problem. *Clin. Genet.* **69**, 105–117 (2006).
21. J. Paredes, S. Sims-Lucas, H. Wang, W. Lu, B. Coley, G. K. Gittes, C. M. Bates, Assessing vesicoureteral reflux in live inbred mice via ultrasound with a microbubble contrast agent. *Am. J. Physiol. Renal Physiol.* **300**, F1262–F1265 (2011).
22. M. J. Anslow, A. J. Bodnar, D. M. Cerqueira, D. Bushnell, B. E. Shrom, S. Sims-Lucas, C. M. Bates, J. Ho, Increased rates of vesicoureteral reflux in mice from deletion of Dicer in the peri-Wolffian duct stroma. *Pediatr. Res.* **88**, 382–390 (2020).
23. D. Narla, S. B. Slagle, C. M. Schaefer, D. S. Bushnell, P. Puri, C. M. Bates, Loss of peri-Wolffian duct stromal Frs2α expression in mice leads to abnormal ureteric bud induction and vesicoureteral reflux. *Pediatr. Res.* **82**, 1022–1029 (2017).
24. I. J. Murawski, R. W. Maina, D. Malo, L. M. Guay-Woodford, P. Gros, M. Fujiwara, K. Morgan, I. R. Gupta, The C3H/HeJ inbred mouse is a model of vesico-ureteric reflux with a susceptibility locus on chromosome 12. *Kidney Int.* **78**, 269–278 (2010).
25. M. Yoshiyama, J. R. Roppolo, M. Takeda, W. C. de Groat, Effects of urethane on reflex activity of lower urinary tract in decerebrate unanesthetized rats. *Am. J. Physiol. Renal Physiol.* **304**, F390–F396 (2013).
26. K. E. Andersson, R. Soler, C. Fullhase, Rodent models for urodynamic investigation. *Neurourol.Urodyn.* **30**, 636–646 (2011).
27. P. Uvin, W. Everaerts, S. Pinto, Y. A. Alpizar, M. Boudes, T. Gevaert, T. Voets, B. Nilius, K. Talavera, D. De Ridder, The use of cystometry in small rodents: A study of bladder chemosensation. *J. Vis. Exp.* **2012**, e3869 (2012).
28. H. Ito, A. E. Pickering, Y. Igawa, A. J. Kanai, C. H. Fry, M. J. Drake, Muro-Neuro-Urodynamics; a review of the functional assessment of mouse lower urinary tract function. *Front. Physiol.* **8**, 49 (2017).
29. C. A. Maggi, B. Conte, Effect of urethane anesthesia on the micturition reflex in capsaicin-treated rats. *J. Auton. Nerv. Syst.* **30**, 247–251 (1990).
30. C. J. Fowler, D. Griffiths, W. C. de Groat, The neural control of micturition. *Nat. Rev. Neurosci.* **9**, 453–466 (2008).
31. F. Sato, S. Tsuchihashi, W. Nakamura, H. Eto, LD50(30)s and daily death distributions of whole or partial body irradiated mice. *J. Radiat. Res.* **13**, 100–108 (1972).
32. J. Schindelin, I. Arganda-Carreras, E. Frise, V. Kaynig, M. Longair, T. Pietzsch, S. Preibisch, C. Rueden, S. Saalfeld, B. Schmid, J. Y. Tinevez, D. J. White, V. Hartenstein, K. Eliceiri, P. Tomancak, A. Cardona, Fiji: An open-source platform for biological-image analysis. *Nat. Methods* **9**, 676–682 (2012).

Acknowledgments: We thank all the members of the Laboratory of Ion Channel for helpful discussion. **Funding:** This research was supported by the following grants: KU Leuven Research Council, grant C1-TRPLe (T.V. and W.E.); Flemish Institute for Biotechnology (VIB), unrestricted grant (T.V.); Research Foundation-Flanders (FWO), research grant G0B4718N (T.V. and W.E.); and Research Foundation-Flanders (FWO), clinical research fellowship (D.D.R. and W.E.). **Author contributions:** J.F., H.D.B., and T.V. conceptualized and designed the experiments; acquired, analyzed, and interpreted data; and wrote the manuscript. T.V. wrote custom analysis software and supervised the project. R.R. helped with experiment design and acquired and analyzed data. A.S. performed data analysis and interpretation and wrote custom analysis software. D.D.R. contributed to conceptualization and editing of the manuscript. W.E. aided in experiment design, data interpretation, and editing of the manuscript. G.V.V. conceptualized and designed experiments and aided in editing of the manuscript. **Competing interests:** The authors declare that they have no competing interests. **Data and materials availability:** All data needed to evaluate the conclusions in the paper are present in the paper and/or the Supplementary Materials. Custom analysis software was written in Igor Pro and is made publicly available, including a reference manual and small datasets for demoing purpose, through GitHub: https://github.com/LICRTV/videocystometry. Additional data related to this paper may be requested from the authors.

Submitted 25 March 2021
Accepted 8 June 2021
Published 23 July 2021
10.1126/sciadv.abi6821

Citation: J. Franken, H. De Bruyn, R. Rietjens, A. Segal, D. De Ridder, W. Everaerts, T. Voets, G. Vande Velde, X-ray videocystometry for high-speed monitoring of urinary tract function in mice. *Sci. Adv.* **7**, eabi6821 (2021).

ScienceAdvances

X-ray videocystometry for high-speed monitoring of urinary tract function in mice

Jan FrankenHelene De BruynRoma RietjensAndrei SegalDirk De RidderWouter EveraertsThomas VoetsGreetje Vande Velde

Sci. Adv., 7 (30), eabi6821. • DOI: 10.1126/sciadv.abi6821

Science Advances (ISSN 2375-2548) is published by the American Association for the Advancement of Science. 1200 New York Avenue NW, Washington, DC 20005. The title *Science Advances* is a registered trademark of AAAS.